Available online at www.sciencedirect.com

ScienceDirect

Scripta Materialia 93 (2014) 12–15

Scripta MATERIALIA

www.elsevier.com/locate/scriptamat

Deformation and crack mechanisms of nanotwinned cadmium telluride under cyclic nanoindentations

Zhenyu Zhang,[a,*] Nengdong Duan,[a] Bo Wang,[a] Yanxia Huo,[a] Bi Zhang,[a,c] Xianzhong Zhang[a] and Fei Ye[b]

[a] *Key Laboratory for Precision and Non-Traditional Machining Technology of Ministry of Education, Dalian University of Technology, Dalian 116024, People's Republic of China*

[b] *School of Materials Science and Engineering, Dalian University of Technology, Dalian 116024, People's Republic of China*

[c] *Department of Mechanical Engineering, University of Connecticut, Storrs, CT 06269, USA*

Received 2 July 2014; revised 18 August 2014; accepted 18 August 2014
Available online 3 September 2014

The surface energies of monocrystalline (mc) and nanotwinned (nt) cadmium telluride (CdTe or CT) crystals, calculated using molecular dynamics simulations, are 435.08 and 381.8 mJ m^{-2}, respectively. A crack of mc-CT is induced at the second loading cycle, whereas nt-CT with both twin boundaries (TBs) shows a crack at the lower TB under the third unloading condition. However, nt-CT with three TBs is free from cracks after 10 cyclic loading–unloading indentations, due to the combined effect between the hardening and softening nanotwins.

Keywords: Cyclic indentation; Crack; Nanotwinned deformation; CdTe; Molecular dynamics

Nanocrystalline metals exhibit higher strength, up to five times that of their coarse-grained counterparts, as described by Hall–Petch equation [1–4], but suffer from significantly diminished ductility [5]. Nanotwinned (nt) copper (Cu) presents a combination of ultrahigh strength and good ductility [6]. It can have strength 10 times that of its coarse-grained counterparts, while still retaining good ductility. Ductility is significantly different between nanocrystalline and nt metals with decreasing grain sizes. For this reason, nt materials are being increasingly studied for their potential applications [5,6]. However, the fundamental mechanisms of ductility for nt materials under cyclic loading conditions are not well understood.

Recently, we reported the nt structure of semiconductors, such as cadmium zinc telluride (CdZnTe or CZT) and mercury cadmium telluride (HgCdTe or MCT). Both CZT and MCT showed higher hardness up to 100 times that for their monocrystalline counterparts, while remaining their ductility, which was evidenced by performing 100 cyclic nanoindentations without crack formation [7–9]. Therefore, it is necessary to explore the fundamental mechanism of ductility for nt semiconductors, under cyclic loading conditions.

In this study, the deformation and crack mechanisms of nt cadmium telluride (CdTe or CT) under cyclic nanoindentations are investigated, using molecular dynamics (MD) simulations.

Both nt-CT MD models are proposed to elucidate deformation and crack mechanisms of the nt semiconductors under cyclic nanoindentations, using individual nanotwins. The thickness of a twin denotes the spacing between adjacent twin boundaries (TBs), hereinafter referred to as λ [6]. The maximum hardness of nt-CT is predicted by MD simulations when λ is ~16 nm [10], above which the hardness is predicted by the Hall–Petch equation; otherwise it obeys the reverse Hall–Petch relation. This means that when $\lambda > 16$, the hardening effect of nt-CT dominates, but when $\lambda < 16$, the softening effect prevails. According to experimental results [7–9], nt-CZT and nt-MCT show a repeating pattern, consisting of a twin showing the hardening effect followed by one or several twin lamellae, which exhibit ultrahigh hardness and high ductility. As a result, both nt-CT include a hardening twin with $\lambda > 16$ nm. One nt-CT has a softening twin with $\lambda < 16$ nm, but the other does not. Both nt-CTs are designated in terms of thicknesses of lamellae sequencing from top to bottom. One is nt 5.6–17.9–5.6, and the other is nt 5.6–17.9–7.8–5.6. The nt 5.6–17.9–5.6 model is 31.6 nm in length, 13.4 nm in width and 29.8 nm in height, consisting of 372,000 atoms. Correspondingly, the nt 5.6–17.9–7.8–5.6 model is 31.6 nm long, 13.4 nm wide and 36.9 nm high, and includes 475,200 atoms. For comparison [11], a monocrystalline (mc) model of CT with both the same dimensions and

* Corresponding author; e-mail: zzy@dlut.edu.cn

http://dx.doi.org/10.1016/j.scriptamat.2014.08.018
1359-6462/

atoms as those of the nt 5.6–17.9–7.8–5.6 model, herein referred to as mc-36.9, has been established. Periodic boundary conditions are applied to all three MD models in both length and width directions. At the bottom, an atomic layer 2 nm thick is fixed for each model. Prior to nanoindentation, each model experiences an isothermal–isobaric (NPT) relaxation for 100 ps at 300 K [11]. A time step of 1 fs is used in all the MD simulations. A displacement-rate-controlled mode is employed during the calculation of the three MD models. Both loading and unloading speed are 20 m s^{-1}, based on the wheel speed used for grinding CZT wafers [12]. A cylindrical indenter of 10 nm in tip diameter is used to perform the nanoindentations. The Stillinger–Weber potential function is applied to calculate the two-body and three-body potentials for CT [13]:

$$W_2 = \varepsilon f_2(r_{ij}/\sigma) \tag{1}$$

$$W_3 = \varepsilon f_3(r_{ij}/\sigma, r_{jk}/\sigma, r_{ki}/\sigma) \tag{2}$$

$$f_2(r) = \begin{cases} A(Br^{-4} - 1)\exp[(r-a)^{-1}], r < a \\ 0, r \geqslant a \end{cases} \tag{3}$$

$$f_3(r_{ij}, r_{jk}, r_{ki}) = h(r_{ij}, r_{ik}, \theta_i) + h(r_{ji}, r_{jk}, \theta_j) + h(r_{ki}, r_{kj}, \theta_k) \tag{4}$$

$$h(r,s,\theta) = \begin{cases} \lambda \exp[v(r-a)^{-1} + v(s-a)^{-1}](\cos\theta + \frac{1}{3})^2, r < a \& s < a \\ 0, otherwise \end{cases} \tag{5}$$

where λ, a, v, ε, σ are 25, 1.8, 1.2, 1.03 eV and 0.251 nm, respectively. Additionally, A is 8.1415, 5.1726 and 7.0496 for the Te–Te, Cd–Cd and Te–Cd two-body potentials, respectively. Correspondingly, B is 0.6671, 0.8807 and 0.6022 [14]. In snapshots of the CT MD models, the blue color represents Te atoms, red indicates Cd atoms, and light yellow marks the TBs.

Figure 1 shows the loading–unloading curves of the mc-36.9, nt 5.6–17.9–5.6 and nt 5.6–17.9–7.8–5.6 MD models induced by cyclic nanoindentations. When the indentation depth varies from 2.8 to 5 nm, resistance to deformation of deformed mc-36.9 model is larger than that of the pristine crystal, as depicted in Figure 1a. Both the nt 5.6–17.9–5.6 (Fig. 1b) and nt 5.6–17.9–7.8–5.6 (Fig. 1c) models exhibit primarily elastic characteristics, and loading–unloading curves after the third cycle are similar between each other, which is consistent with the experimental reports [7–9].

Figure 2a–d shows snapshots of the mc-36.9 at an indentation depth of 46 Å in the second loading, 44 Å in the sixth loading conditions, and two-dimensional (2-D) and three-dimensional (3-D) deformed MD models after the eighth unloading, respectively. Eleven pairs of edge dislocations are formed in Figure 2a, and a crack 1.9 nm long is observed at the bottom along the slip direction. A cell structure emerges in Figure 2b. Twenty-nine edge dislocations are produced and dislocation tangles appear. Cracks form at the corners of the cell, and one crack is located at the bottom. Forty-six pairs of dislocations are induced by the stress generated under cyclic nanoindentations in Figure 2c. A nanometer crystallite emerges, and the cell structure still exists. Cracks distribute at both corners of a cell and another two at the bottom of the MD model.

Figure 3a–d show snapshots of nt 5.6–17.9–5.6 at an indentation depth of 50 Å in the second loading, 22 Å in the third unloading conditions, and 2-D and 3-D deformed MD models after the fourth unloading condition, respectively. Ten pairs of edge dislocations are identified in Figure 3a, and a crack is shown at the junction point between the slip {1 1 1} plane and the fixed layer. Eight pairs of edge dislocations are formed in Figure 3b, and a triangular crack 12.1 nm long appears at the lower TB initiated at the junction point between the slip {1 1 1} planes and the lower TB. Eight pairs of dislocations are found in Figure 3c, and the crack in Figure 3b is further developed, as shown in Figure 3c.

Figure 4a–d show snapshots of nt 5.6–17.9–7.8–5.6 at an indentation depth of 50 Å in the second loading, 22 Å in the third unloading conditions, and 2-D and 3-D deformed MD models after the tenth unloading condition, respectively. Nine, seven and nine pairs of edge dislocations are correspondingly displayed in Figure 4a–c. There is no crack

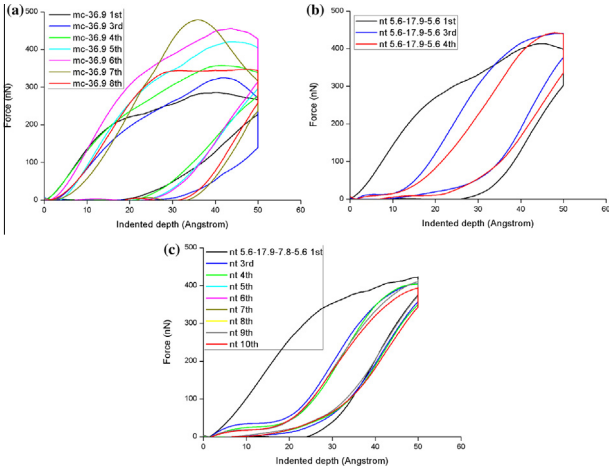

Fig. 1. Loading–unloading curves of the (a) mc-36.9, (b) nt 5.6–17.9–5.6 and (c) nt 5.6–17.9–7.8–5.6 MD models induced by cyclic nanoindentations.

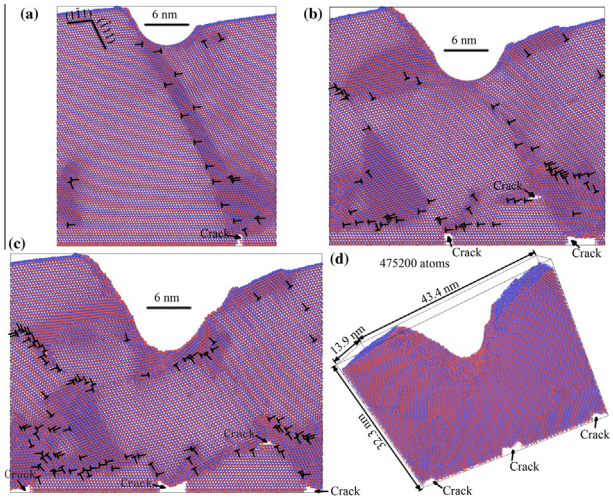

Fig. 2. Snapshots of mc-36.9 at an indentation depth of (a) 46 Å in the second loading, (b) 44 Å in the sixth loading conditions, and (c) 2-D and (d) 3-D deformed MD models after the eighth unloading cycle.